Hindawi Publishing Corporation
International Journal of Rotating Machinery
Volume 2009, Article ID 787145, 11 pages
doi:10.1155/2009/787145

Research Article

Study of Sweep and Induced Dihedral Effects in Subsonic Axial Flow Compressor Passages—Part I: Design Considerations—Changes in Incidence, Deflection, and Streamline Curvature

P. V. Ramakrishna and M. Govardhan

Thermal Turbomachines Laboratory, Department of Mechanical Engineering, Indian Institute of Technology Madras, Chennai, 600036, India

Correspondence should be addressed to M. Govardhan, gova@iitm.ac.in

Received 19 August 2009; Revised 3 November 2009; Accepted 31 December 2009

Recommended by Chunill Hah

This article presents the study of Tip Chordline Sweeping (TCS) and Axial Sweeping (AXS) of low-speed axial compressor rotor blades against the performance of baseline unswept rotor (UNS) for different tip clearance levels. The first part of the paper discusses the changes in design parameters when the blades are swept, while the second part throws light on the effect of sweep on tip leakage flow-related phenomena. 15 domains are studied with 5 sweep configurations (0°, 20° TCS, 30° TCS, 20° AXS, and 30° AXS) and for 3 tip clearances (0.0%, 0.7%, and 2.7% of the blade chord). A commercial CFD package is employed for the flow simulations and analysis. Results are well validated with experimental data. Forward sweep reduced the flow incidences. This is true all over the span with axial sweeping while little higher incidences below the mid span are observed with tip chordline sweeping. Sweeping is observed to lessen the flow turning. AXS rotors demonstrated more efficient energy transfer among the rotors. Tip chordline sweep deflected the flow towards the hub while effective positive dihedral induced with axial sweeping resulted in outward deflection of flow streamlines. These deflections are more at lower mass flow rates.

1. Introduction

Sweep is incorporated to a baseline turbomachinery blade by tilting its stacking axis in relationship to the flow field. This is achieved by linearly translating the aerofoil blade sections from hub to tip for a given sweep angle in such a way that the amount of movement is zero at the hub and highest at the tip.

Three dimensional forward sweep designs have shown increased compressor efficiency and operating range [1–5], higher pressure rise with moderate sweep angles [4], suppression of secondary losses [1, 5, 6], reduced blade loading near the tip leading edge portions [4, 6], and low tip clearance flow blockage [7]. Deliberate use of sweep in subsonic blade rows is found to improve the operating range and efficiency characteristics, while in transonic environment it is due to significant changes in the shock structure to reduce shock-related losses [2, 3]. Leading edge sweep is employed in designs intended to modify the local blade loading conditions. Forward sweep modifies the flow structure in low speed axial compressors by the following: (1) Reducing the blade loading in the frontal area near the tip region, which results in flow near the leading edge becoming more tolerant to the changes in incidence and reduced tip leakage in this area. (2) Modification in the movement of centrifuged blade boundary layer which will not result in accumulation of low energy fluid near tip sections to cause separation and formation of stall cells at lower flow coefficients [1, 4, 5]. Major sweep effects in compressor rotors are thus found above the mid span, particularly near the tip, where the flow leaking from the finite tip gap already has its own influence.

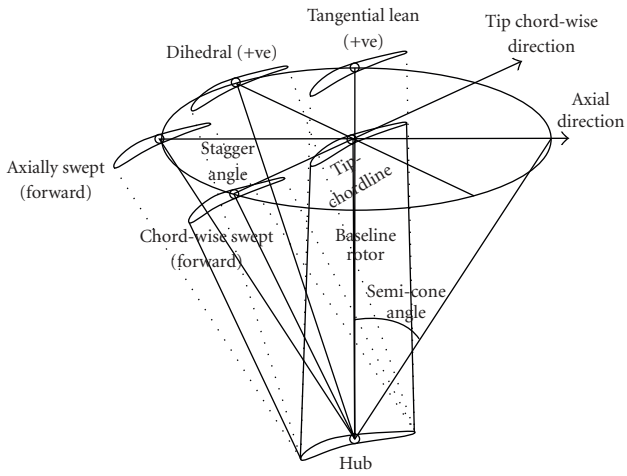

Figure 1: Definitions of various staking line modification schemes and conventions.

Table 1

S. No	Scheme	Code
(1)	Unswept rotor (Baseline)	UNS
(2)	20° Forward sweep (Tip chordline swept)	20° TCS
(3)	30° Forward sweep (Tip chordline swept)	30° TCS
(4)	20° Forward sweep (Axially swept)	20° AXS
(5)	30° Forward sweep (Axially swept)	30° AXS

In low aspect ratio machines, large variations in blade speed and flow conditions are seen from hub to tip (in the meridional plane). Flow conditions are further modified by the presence of hub and casing endwalls. Theories based on infinite span blades would invariably be different in such cases. Streamline twist [8, 9] and spanwise redistribution of flow [4, 7] are reported with sweep in such low aspect ratio configurations. Starting from lifting line theory, nearly all the blade design procedures (axisymmetric flow assumption followed by finding a blade-to-blade solution for each axisymmetric stream surface) are not legitimate when the blades are swept. This needs some of the design aspects to be thoroughly confirmed when the blades are swept. Differences arise in terms of effective flow incidences, meridional velocity distribution, and effective blade angles if the blade stacking is highly three dimensional. Smith and Yeh [8] have shown that designing a swept blade on sections defined by the axisymmetric stream surfaces generated by the throughflow calculation methods is not correct. Instead, sections perpendicular to the stacking axis must be chosen for the design. Equations for aerodynamic sweep (λ), projected chord and projected blade spacing would provide the important parameters as well as the correct solidity to use when designing the blade shape in such cases. In turbine cascade studies, Pullan and Harvey [10] showed that for a fixed value of meridional velocity, in order to maintain a fixed lift coefficient, the pitch-chord ratio must be reduced when the blades are swept. This means increased wetted area of the blades to increase the profile loss. Even with the same pitch-chord ratio and the same number of blades, sweeping/bowing would increase the blade surface area, which was reported to cause loss of pressure rise and the efficiency toward high mass flow rates on account of increased friction losses on the blade surfaces [11].

Since translating the blade sections changes the axial distance between the swept rotor and the succeeding radial stator, a considerable amount of stage matching needs to be justified because, for instance, increasing gap between rotor and stator has its own effects in terms of flow mixing, pressure loss, and modified incoming flow angles as received by the stator. Orientation of wake leaving the rotor also differs for various sweep/dihedral configurations which results in incoming flow distortion effects to the stator vanes.

In the present study, flow phenomena in a low-speed axial compressor rotor-stator stage are considered for studying the effects of rotor sweeping. Effects of the same on the overall (global) performance parameters like total pressure coefficient, axial velocity distributions, losses in the rotor passages, and so forth, from this study were reported earlier in detail [12]. The objective of the present paper is to present the internal flow phenomena in a detailed fashion.

The first part of the paper addresses some of the issues related to changes in design aspects when the blades are swept, while the second part throws light on the effect of sweep on tip leakage flow-related phenomena.

2. Sweep Configurations

A variety of terms have been used to describe stacking line modifications (e.g., sweep, lean, dihedral, bow and skew) by the researchers. The conventions followed in this present work are illustrated through Figure 1. When the aerofoil sections are tilted in axial and tip chordwise directions of the blade, they are referred as "axially swept" and "tip chordline swept", respectively. Design of swept blades is done in such a way that the passage area distribution qualities of unswept rotor in terms of camber, tip clearance, and solidity are preserved.

It is evident from the literature that the application of forward sweep is disappointing near the casing due to increased tip-clearance losses while positive dihedral reduces tip clearance and hub corner losses (Gallimore et al. [13]). Based on the results from the literature [4–6, 13], it was contemplated that better 3D stacking scheme would be the combination of forward tip chordline sweeping and positive dihedral, which turns out to be "axial sweeping". Thus, the 3D blade stacking schemes chosen for the present study are shown in Table 1.

Table 2: Specification of the compressor stage.

Rotational speed	1950	rpm
Design mass flow rate	2.725	kg/s
Number of rotor blades	12	—
Casing diameter	400	mm
Hub diameter	200	mm
Mean chord (rotor and stator)	75	mm
Axial tip chord (rotor)	50.09	mm
Aspect ratio based on mean chord (rotor and stator)	1.33	—

3. Computational Details

3.1. Computational Model. The computational domain consists of a rotor followed by a stator row with specifications mentioned in Table 2. The rotor was designed to give a forced vortex flow at constant exit absolute flow angle, and a specific work of 425 m^2/s^2 at the designed flow coefficient of 0.60.

The important considerations for the blade design were the following: It should have a high camber so that a thick boundary layer will develop near the trailing edge. Chord length should preferably be constant along the span so that using the same profile the thickness will remain constant from the hub to the tip. Stator design was done with the criterion that absolute flow angle leaving the stator is axial. The stator used in conjunction with these rotors is radial (unswept) in all the cases. Positioning the stator downstream to the rotor is done in such a way that the axial gap between rotor TE and stator LE at hub is (37.5 mm) half the mean chord of the rotor (75 mm). This axial gap is decided after observing the (1) wake pattern coming out of the rotor passage (via contours of total pressure) (2) variation of the absolute flow angle at this streamwise station. The criterion used is that the wakes should be well mixed out so as to have minimal effect on the stator vanes.

Blade geometry creation and grid generation are done using commercial software ANSYS ICEMCFD 10.0. CFD simulation and flow analysis are done using commercial CFD code ANSYS® CFX 11.0. Hexahedral grids were employed with finest mesh near the walls and within the tip gap for better mesh resolution. The solution was second-order accurate. Coupled solver was used for the simulations. Various turbulent models were tried for the flow modelling. Standard k-ω and SST k-ω turbulence models are found to predict the flow physics closer to the experiments. A standard k-ω turbulence model is used for the simulations with automatic wall function treatment at walls with less computational effort. The results obtained with these two turbulence models are compared with the experimental results [4]. Grid independency study was also conducted and the mesh size is optimized to about 700,000 mesh elements for the rotor and 450,000 elements for the stator. Details of the flow domain with given boundary conditions is shown in Figure 2.

The fluid chosen was air at 25°C and is set incompressible by making density independent of temperature and pressure. Velocity and flow direction in the stationary frame of reference were specified at the rotor inlet, whereas uniform static pressure was specified at the stator (domain) outlet. Hub and blade were specified as stationary walls in rotating frame of reference, whereas the rotor casing wall was a counter-rotating wall with respect to the flow within the rotor. A frozen rotor interface was chosen for the rotor—stator frame change interface. Computations are carried out for five-flow coefficients from minimum $\phi = 0.50$ to higher $\phi = 0.71$ including the design $\phi = 0.60$.

Nondimensionalised streamwise location "x" for the stage is defined in such a way that $x = 0$ corresponds to the domain inlet and $x = 2$ corresponds to stator (domain) outlet. Rotor-stator interface is at $x = 1$. All the measurements corresponding to the rotor inlet and rotor exit are made on planes which are parallel to the domain inlet and are located at $x = 0.03$ and $x = 1.11$ (L_1 and L_2 in Figure 2), respectively.

3.2. Experimental Validation. Figure 3 compares the spanwise variation of circumferentially averaged total pressure coefficient ($\overline{\psi}_o$) from present CFD study with the data measured from the experiments [4]. Both the experimental data and CFD plot correspond to a tip gap of τ/ch= 0.007 for the flow coefficients 0.54 and 0.71. Spanwise variation graphs of almost all the primary parameters of interest (pressure, velocities, and flow angles, etc.) were validated in similar way with the experimental results [4]. CFD results with the unswept rotor are in good agreement with experiments while computations over predicted the pressure coefficient near the tip regions in the case of 20°TCS rotor due to low estimation of tip leakage related loss by the flow solver.

4. Results and Observations

Validity of changing the sweep of a blade without redesigning the aerofoil sections has been a subject of debate owing to the changes in effective inlet velocities, incidences, and location of maximum thickness caused by sweep. While many studies incorporated sweep directly to the baseline design [1–6, 13], some researchers redesigned the blade sections to alleviate the influence of nonsweep parameters (such as change in effective incidences, loading, etc.) in studying the effect of sweep. Meridional velocity, inlet, and exit tangential velocities and hence the flow angles are typically preserved while redesigning the swept blade sections for comparison purposes [10]. Fundamental to this redesigning process is to understand how sweeping alters some of these design parameters.

4.1. Change in the Incidence with Sweep. The baseline rotor blade is designed for certain flow incidences varying along the span. However, incidences observed from the computations are little less than the designed values. The spanwise variations of design and observed parameters are given in Table 3. The incoming flow angle as received by the blade alters when the blades are swept. As a result, the effective incidence in swept rotors is different from the one

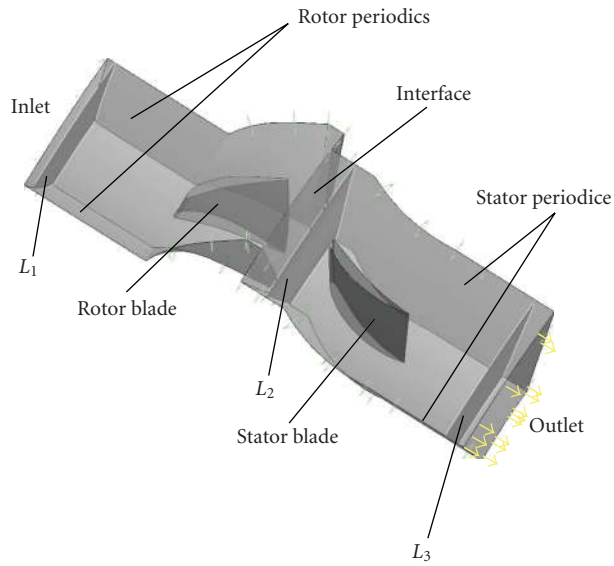

Figure 2: Flow domain with the given boundary conditions.

Table 3: Spanwise Variation of Parameters.

Span	Designed			Observed (At design ϕ)	
	Incidence	stagger	S/ch	Incidence	Deflection
(Tip) 100	−13.00	44.5	1.40	−16.30	15.3
80	−11.00	39.5	1.29	−13.50	17.1
60	−9.00	35.0	1.12	−10.85	20.5
40	−6.75	28.5	0.98	−8.15	25.2
20	−4.20	21.5	0.80	−5.25	29.3
(Hub) 0	−2.00	14.5	0.65	−2.70	32.2

with unswept rotor. The extent of incidence change relative to the observed incidence in the unswept rotor at design flow coefficient [$\Delta i = i - i_{\mathrm{UNS}^*}$] is plotted along the span in Figure 4. Incidence angles are measured at a location 4 mm ahead of the rotor LE. These differences in the incidence angles are considered for better depiction of the incidence changes with sweeping as well as with the mass flow rate variations.

When the blades are given forward sweep they are found to receive the flow at lower incidences. This is true all over the span for axial sweeping while tip chordline sweeping is observed to result in little higher incidences below the mid span. The effective dihedral in AXS rotors on flow incidence is evident from these observations. Change in incidence is more uniform for the AXS rotors along the span. The differences and spanwise variations are less at higher flow coefficient and they are amplified as the mass flow rate is reduced. That is, at lower flow coefficients, the incoming flow incidence is minimum with forward sweeping. This is beneficial, as higher incidence near the tip is threat for stall at low flow coefficients. Tip chordline sweeping resulted in lowering the incidence above the mid span and increasing the incidence below the mid span. This is beneficial at choking mass flow rates near the hub regions, where too low incidences are to be prevented. Among the two swept rotors, AXS rotor exhibited little higher incidences near the tip regions when compared with that of the TCS rotor at higher flow coefficients. However, as the mass flow rate is reduced, opposite effect is observed. This tendency of the AXS rotor is beneficial, as the incidence angle is critical in these regions at the near stall mass flow rates.

Smith and Yeh [8] have shown that the vorticity of a swept blade contains an axial component which according to Squire and Winter [14] will induce a secondary flow in a plane perpendicular to the machine axis. The effect of this secondary flow on the swept back blades is to increase the incidence [8]. The opposite will be the effect when the blades are swept forward. The present results are in conformity with these effects.

4.2. Flow Deflection and Total Pressure Coefficient. When compared with the unswept rotor, low flow turning is observed in axially swept rotor passage all along the span (Figure 5). TCS rotor is found to improve little flow turning below the mid span.

It is to be noted that following the arguments of Lewis and Hill [15] and Smith and Yeh [8], the stream surface views

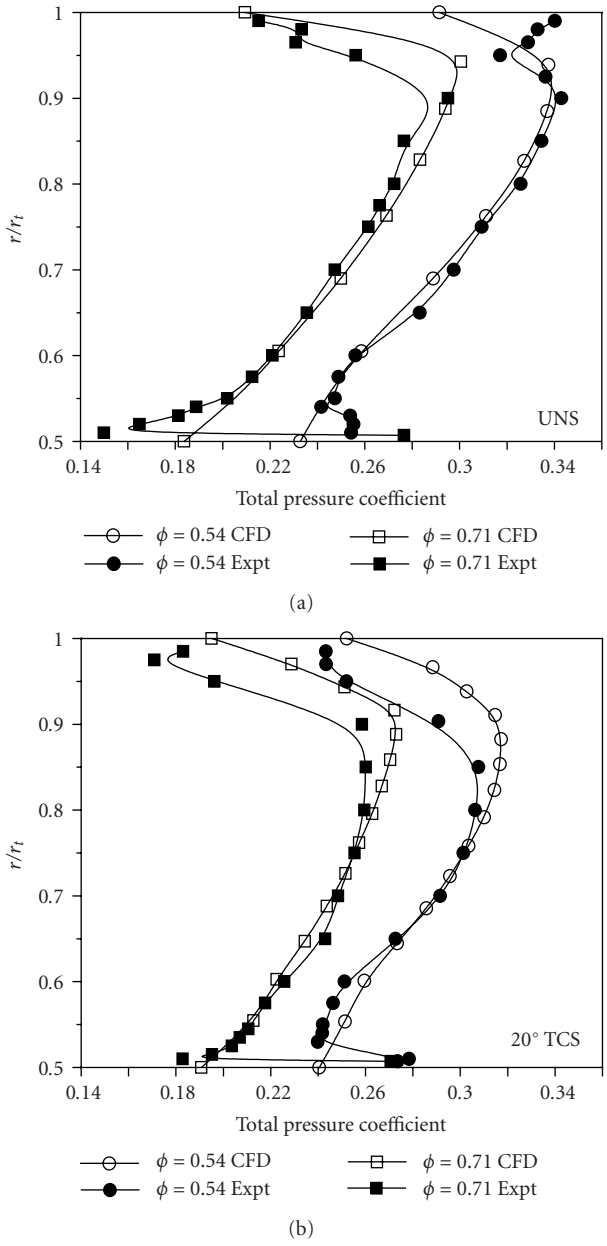

Figure 3: Variation of total pressure coefficient at the rotor exit.

the blade shapes at a sweep angle λ, as it crosses the blade. The flow direction makes an angle with the meridional direction, which has the axisymmetric stream surface cutting across the "apparent" blade chord of *ch/cos* λ. It is in this cross-section that the correct fluid outlet angle can be calculated. The differences between the conventional method of using the blade shape viewed on a surface parallel to the axis to calculate the fluid deflection angle versus the correct method of using the actual blade shapes at the sweep angle (the projection method) shows that the conventional methods predict a smaller fluid outlet angle or greater fluid turning than the projection method. Considering this effect, all the outlet flow angles were measured on a plane which is "blade aligned," that is, plane which makes sweep angle with respect to the axial direction in alignment with the blade trailing edge. While this roughly confirms to the projection method, any differences would essentially over estimate the turning. Thus the actual flow turning could still be little lesser with the swept rotors than that predicted in these graphs.

At the minimum flow coefficient, AXS tip sections are found to turn flow 5° less than that of UNS rotor while it is 3° in the case of TCS rotor. At other mass flow rates and at the lower span heights these differences in the flow turning are less. The high deflections found with the UNS rotor at this flow coefficient near the casing are due to the flow overturning caused by the separated flows at these regions.

These flow separations on the suction surfaces of the respective blades are shown with streamline patterns in Figure 6. It was already mentioned that the primary objective of sweeping the blade is to prevent the centrifuged boundary layer flow on the rotor suction surface from getting accumulated near the casing. Natures of these separations, as modified by the blade sweep are shown in Figure 6. According to Gbadebo et al. [16], for corners without tip clearance, the presence of three dimensional separations appears to be universal; the challenge for the designer is to limit the loss and blockage produced. For well-designed blade passages, the 3D separation may sometimes be small enough to ignore or overlook. Figure 6 clearly shows that in the case of UNS rotor, boundary layer fluid from various radial locations on the blade migrated towards the tip, and separated from the blade in these regions to turn into tip corner stall cells. This migration is not vigorous in both the swept rotors. With tip chordline sweeping, migratory boundary layer fluid is suppressed in the regions above the mid span, before reaching the tip to form the low energy stall cells. This fluid is separated from the blade at a lower radius and the separation is not severe when compared with that of UNS rotor. With AXS rotor, only the boundary layer fluid from small portions of the blade near the TE is migrated upwards and separated near the blade tip. This separation in AXS rotor did not result in any flow rolling up similar to the separation vortex, which is observed with the other two rotors with different intensities. These variations elucidate the differences in the flow deflections near the tip sections at this flow coefficient (ϕ = 0.50). Even at a little higher flow coefficient of ϕ = 0.54, these streamline patterns on the suction surfaces and the separation phenomena in the respective rotors are found to be similar [12].

Spanwise variation of the total pressure coefficient across the rotor is plotted against radius in Figure 7. TCS rotors are found to produce lower pressure rise for most of the span except near-hub regions, where slightly higher pressure rise is observed with these rotors. AXS rotors developed higher pressure rise all over the span, especially by 20°AXS rotor, while it is limited to regions above the mid span for 30°AXS rotor. This higher pressure rise seen with AXS rotors in spite of low flow turning indicates efficient energy transfer with AXS rotors, which is evident from the relative stagnation pressure loss coefficient (Y_{rel}) values in Figure 8. This figure shows the variation of Y_{rel} over the mass flow range. UNS rotor showed highest loss coefficient values at all mass flow

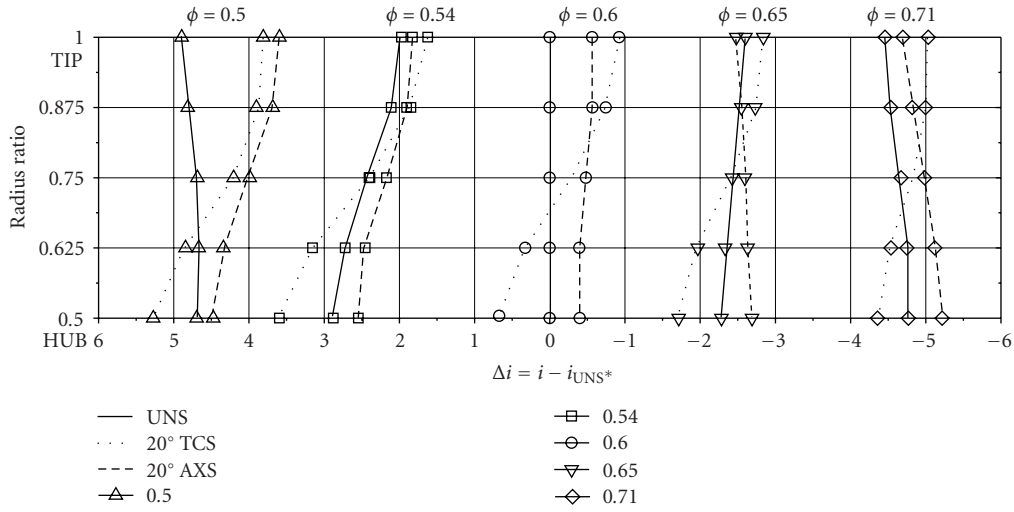

Figure 4: Change in incidence.

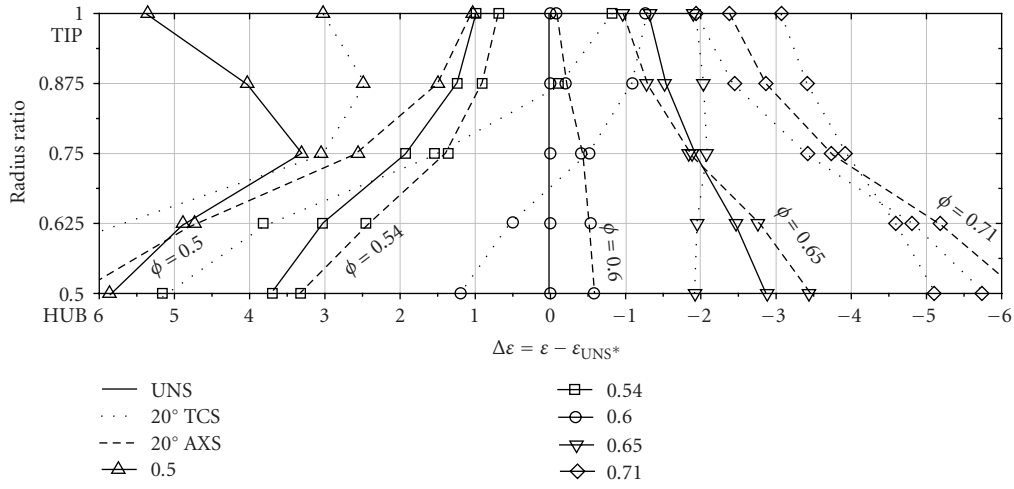

Figure 5: Change in deflection.

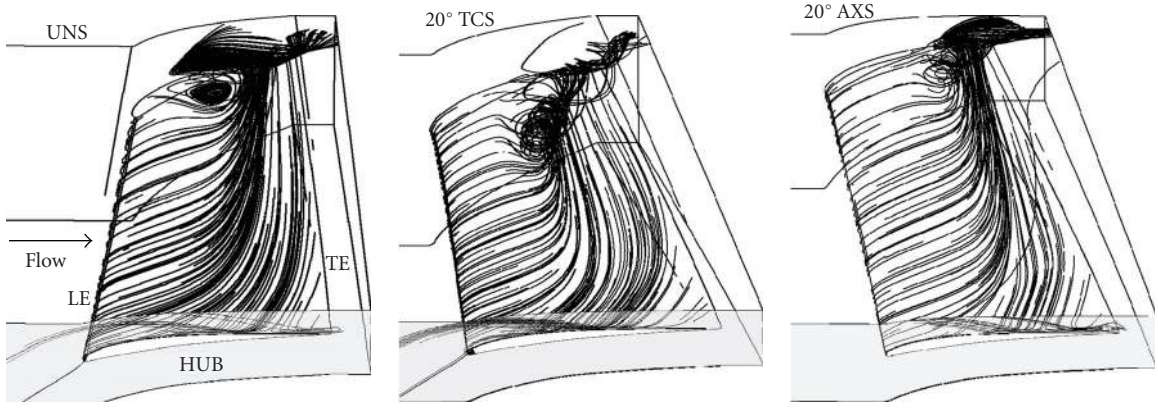

Figure 6: Streamline patterns in the suction surface flow separated regions in various rotors.

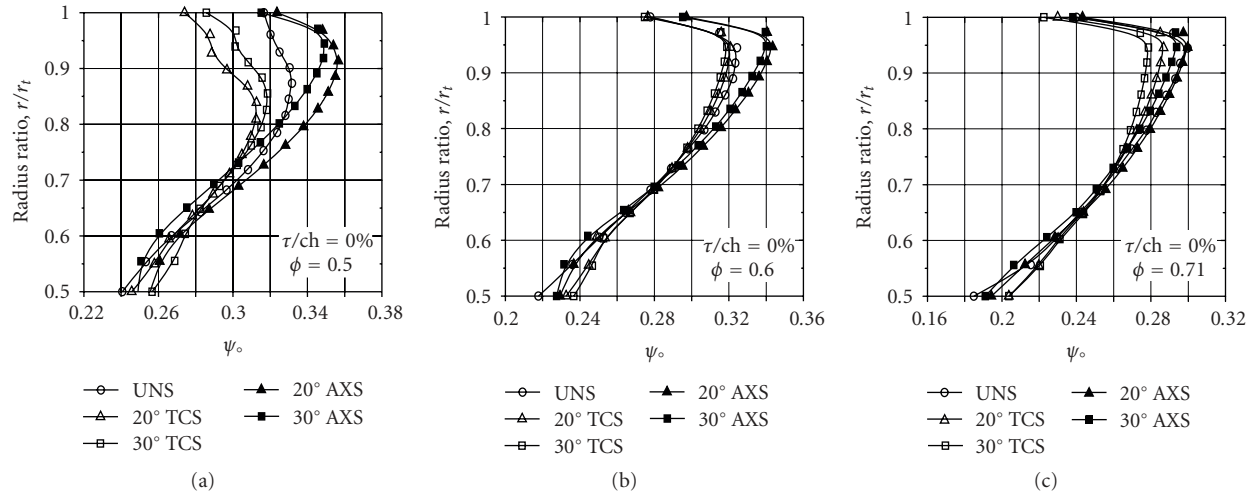

Figure 7: Variation of total pressure coefficient at the rotor exit.

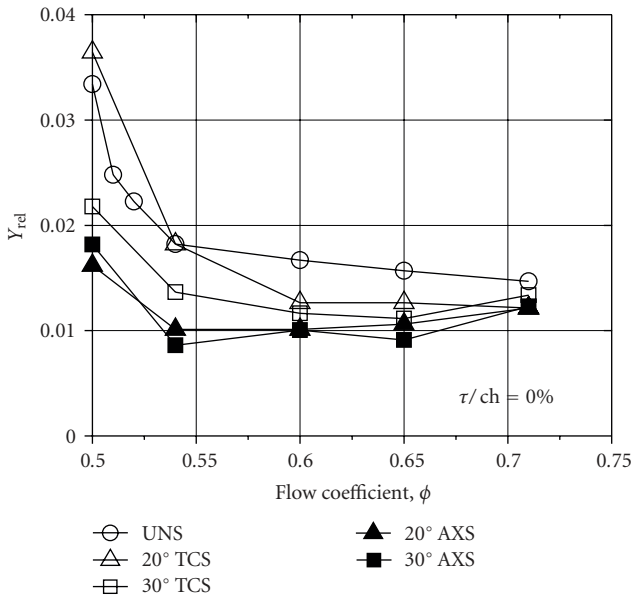

Figure 8: Stagnation pressure loss coefficient across rotor versus ϕ.

rates. AXS rotors showed the lowest loss while TCS rotors have moderate loss coefficient values.

4.3. Streamline Curvature. The radial equilibrium equation may be written as

$$F_r + \frac{1}{\rho}\frac{dp}{dr} = \frac{C_u^2}{r} + \frac{C_m^2}{r_c}, \tag{1}$$

where, F_r is the radial blade force per unit mass of fluid. In a conventional radial blading, $F_r = 0$ and the flow is assumed to remain on the axisymmetric stream surface (r_c = infinite) and the radial equilibrium equation thus reduces to

$$\frac{1}{\rho}\frac{dp}{dr} = \frac{C_u^2}{r}. \tag{2}$$

This equation shows that the radial pressure gradient is balanced by the centrifugal forces. However, for a blade row in a parallel annulus, stream surface twist will only be zero if the flow is free vortex. Otherwise twist will be induced by either shed vorticity (which must produce opposite spanwise velocities on the two blade surfaces at the trailing edge) or by secondary flow arising from inlet vorticity. Flow with large spanwise velocity causes the stream surfaces to undergo twisting. When the blades are truly radial, the effect of blade force on the flow in the radial direction due to the circumferential pressure gradients is nil. But as some amount of lean is inevitable for any axial machine owing to the difference in hub and casing diameters, a little amount of radial blade force would affect the streamline curvature even in a conventional baseline blade passage. On the other hand, with sweep/lean, the spanwise direction of the blade will not be perpendicular to the direction of flow, which will introduce additional radial blade force F_r due to which streamlines acquire additional curvature. The direction of curvature will be different on suction and pressure surfaces depending on the type of sweep/lean employed, as a result of which the original stream surface made under the assumption of radial equilibrium will be twisted.

In addition to these effects, in the case of a forward swept rotor with moderate variation of axial chord along the span, it is the leading edge at the tip which receives the incoming fluid first, whereas it is the leading edge at the hub in the case of UNS or backward swept rotors. Energy transfer and hence blade loading starts at these locations and results in a radial pressure gradient, in addition to already existing spanwise pressure gradient and the blade force F_r introduced by the blade sweep. This causes the flow streamlines in these rotors to undergo further deflections.

In order to assess the streamline curvature, pitch angle [$\beta = \tan^{-1}(C_r/C_m)$] variations are observed at different spanwise locations along the blade passage (Figure 9). Selection of the spanwise locations is such that two sections

very close to the endwalls, one at the mid span height and one section each in the upper half and lower half of the mid span are considered. As the definition implies, pitch angle of the flow streamlines at a given point depends upon the local radial and axial (meridional) velocity components. Streamlines are perfectly axisymmetric, when the radial component of velocity is zero. Dotted line in the graphs indicates zero pitch angles as the case of perfect axisymmetric streamline trend. Any deviation, above or below from this line is an indication of flow having a certain pitch angle. More positive (outward) is the radial velocity, more is the flow towards the casing and opposite is the case with negative (inward) radial velocities. In a nut shell, any curve joining the variations in pitch angle would indirectly indicate the mean trend of streamlines at that given spanwise location.

Before observing the pitch angle variations, axial velocity distribution is surveyed for various rotors at rotor exit for better understanding of the streamline trend (Figure 10). Design of the blading is such that axial velocity is constant from hub to tip. However, variation is seen at all flow coefficients with low axial velocity at hub and increasing towards the higher radii. As the mass flow is reduced, the velocity profile would generally skew, with a larger reduction in axial velocity towards the hub than at the tip.

This axial velocity skew is normally accompanied by diffusion of the root and acceleration of the tip stream tubes across the blade row, which results in an outward radial shift in the stream tube mean radius for both the hub and tip. The greater than unity AVR at the tip section would result in a decreased loss coefficient and deviation angle, both of which would tend to make the tip sections more effectual [17]. This kind of behaviour is significant in AXS rotors.

TCS rotors exhibited higher values of axial velocity near the hub and lower values near the casing when compared with the UNS rotor. Axial velocity can be interpreted in two ways. Higher axial velocities could indicate low flow turning; or as axial velocity is measure of mass flow rate, this might imply the tendency of the TCS rotors to deflect the flow more towards the hub regions. Since it is already observed that flow turning in TCS rotors below the mid span is little higher, it is the tendency of TCS rotors to deflect the flow towards the hub regions resulting in higher axial velocities in these regions. On the other hand, AXS rotors demonstrated the opposite behavior indicating flow deflections towards casing. This behaviour is more predominant when the sweep angles are increased. This phenomenon resulted in higher pressure rise at higher radii with AXS rotors, as the increased flow above the mid span together with low flow turning in these regions tend to minimize the secondary flows and wake-related losses. All the differences in the axial velocity distributions amongst the rotors are reduced as the mass flow rate is increased.

Referring back to Figure 9, it confirms the flow deflections by the two-sweep configurations. All the rotors showed inward flow pitch angles at higher radii. These inward pitch angles are caused due to the fact that there can be no flow acceleration normal to the endwall to move the flow streamlines upward. Radial pressure gradient at these regions, which is adverse in nature, causes the inward movement of the streamlines. Effect of sweep on the streamline shift is observed a little away from the endwalls. While AXS rotor showed positive pitch angles in most of the span portions, TCS rotor along with UNS rotor showed inward flow shifts. These effects are suppressed by the presence of inner and outer endwalls. In the case of TCS rotor, there is a little outward radial velocity observed as the blade receives the flow. However, as the flow progresses into the blade passage, it is swiftly deflected towards the hub with high inward radial velocity for this rotor. Highest inward radial velocity

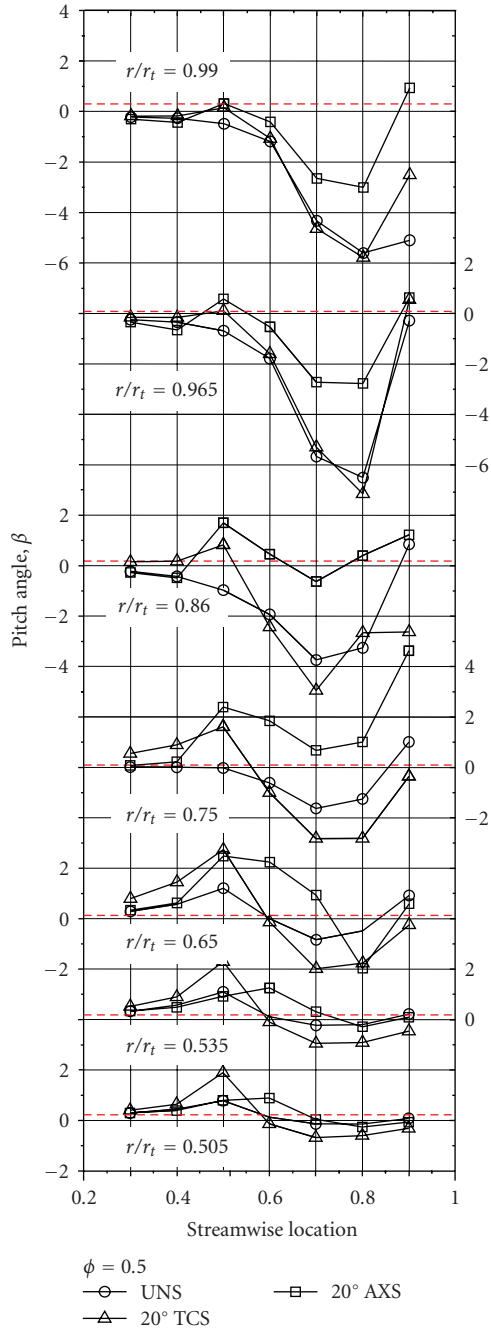

Figure 9: Pitch angle (rad).

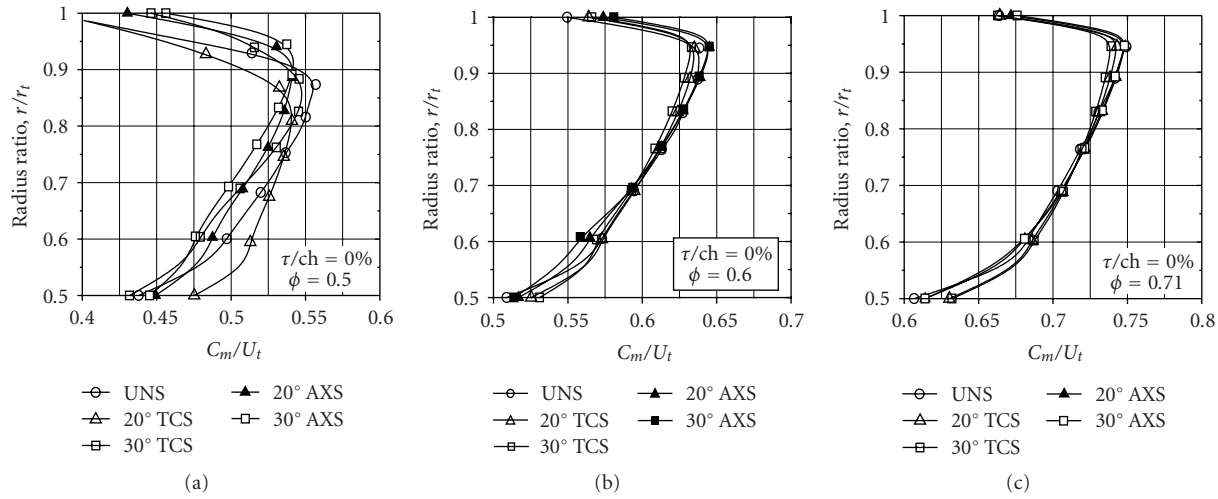

Figure 10: Spanwise variation of axial velocity coefficient at the rotor exit.

observed for the UNS and TCS rotors occurs at about 93% span, while highest casing ward deflection is observed at the mid span with the AXS rotor.

All these differences in the variation of streamline deflections among the rotors will tend to diminish at higher flow coefficients. At low flow coefficients, axial velocity (C_m) is less while radial velocity (C_r) [inward/outward] is observed to be high. At the high flow coefficients, this is opposite. Hence, deflection of flow streamlines due to sweep is more at lower flow coefficients.

4.4. Absolute Flow Angle. The absolute flow angle (α) variation is plotted in Figure 11 at rotor and stator exits. When the mass flow rate is reduced, assuming constant blade angle, the effective absolute flow angle would also reduce. In such case, for the flow to become axial at stator exit, it has to undergo high level of turning in the stator. Hence there is a chance for high residual swirl to remain with the flow at lower flow coefficients. This is what is observed from the plots made at stator exit. Stator is seeing the differences in the flow patterns coming out from different swept rotors. Even at the design flow coefficient $\phi = 0.60$, where α_2 distribution at the rotor exit for various rotors are overlapping, there is a significant difference in α_3 turned by the stator, especially below the mid span.

With TCS rotors, α_3 is observed to be more at lower radii (more axial) and low at the higher radii. This is due to higher mass flow entering the stator at lower radii, from inward flow shift as observed with the TCS rotors. An opposite effect is expected from AXS rotors due to outward flow shift. This is not observed from α_3 graphs owing to the fact that the increased gap between rotor and stator at higher radii due to sweeping is sufficient enough to make the outward deflected flow in AXS rotors to mix and redistribute before entering the stator passage. Hence α_3 distributions with all swept rotors are going inline in the regions above the mid span. The differences in the α_3 distributions are much less at higher flow coefficient.

4.5. Effect of Sweep on Succeeding Stator Vane Passage. The main objectives of the stator installed in succession with the rotor stage are to (1) turn the flow to the required stator outlet angle (α_3) and (2) convert the dynamic energy available at the stator inlet to static pressure. To study the ability of the stator to convert the dynamic pressure available at the rotor exit (stator inlet) to static pressure, "static pressure recovery coefficient, C_{P_rec}" is plotted in Figure 12, which is defined as

$$C_{P\_rec} = \frac{P_3 - P_2}{[P_3 - P_2]_{UNS^*}}. \tag{3}$$

where $[P_3 - P_2]_{UNS^*}$ is static pressure recovered by the UNS rotor at the design flow coefficient. Since the stator is essentially designed for this condition, this value is taken as the reference for normalization. The numerator represents the static pressure recovery across the stator at different mass flow rates for various swept rotor cases.

At all flow coefficients, stators employed with AXS rotors showed lowest C_{P_rec} values. The reason for this could be twofold. It is already seen that AXS rotors exhibited low turning and higher pressure rise at the rotor exit. Hence the majority of the energy is already transferred to the fluid with AXS rotors and the "recoverable dynamic pressure for conversion to static pressure" at the rotor exit is relatively less. Secondly, an appropriately redesigned stator would result in a better match with the swept rotors to effectively recover the available dynamic pressure. Increased axial gap between rotor and stator due to sweeping is also equally influential for the lower C_{P_rec} values. High recovery is observed for the stator when it is employed in conjunction with the UNS rotor. This is much significant at low flow coefficients. It is already observed that the absolute flow angle leaving the stator at higher flow coefficients is nearly 90°. Therefore, at high flow coefficients, the stator effectively turned the flow to leave axially, while the objective to recover the available dynamic head is effectively accomplished at the low flow coefficients.

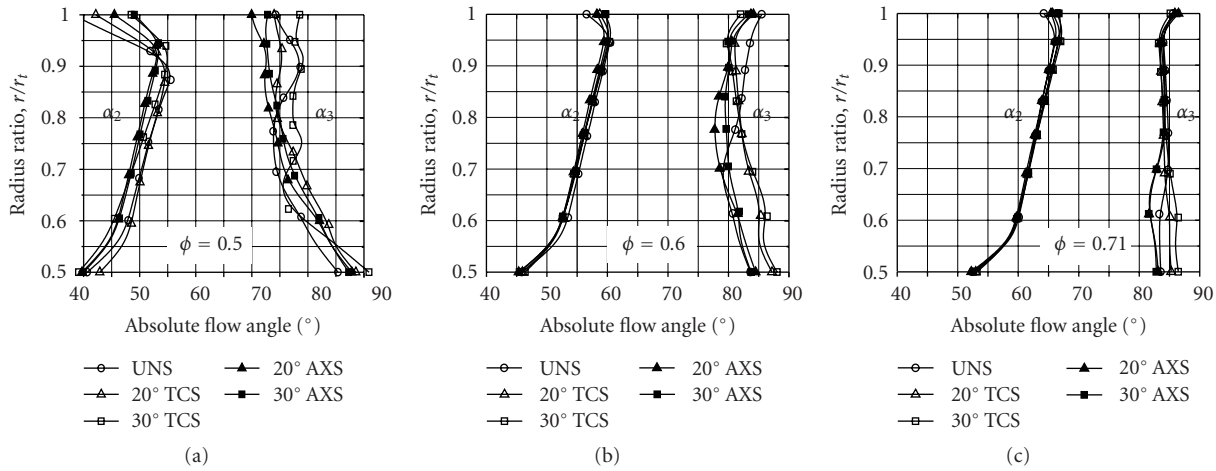

Figure 11: Spanwise variation of absolute Flow angle, α at rotor exit and stator exit.

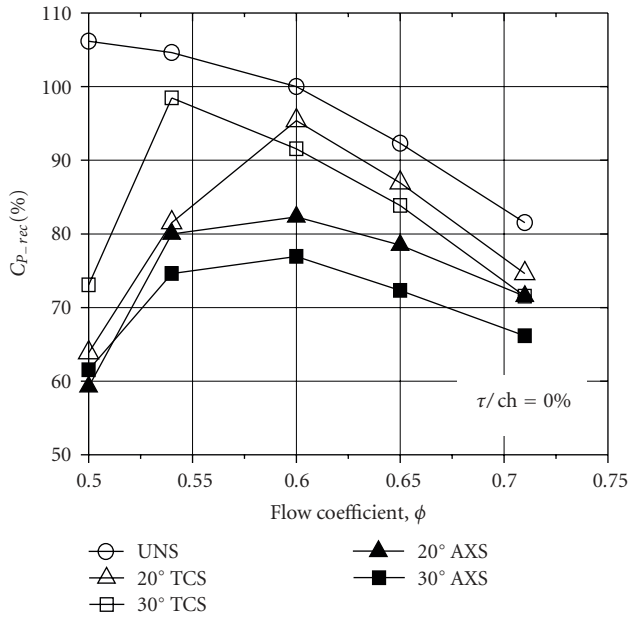

Figure 12: Static pressure recovery coefficient in the stator.

C_{P_rec} is lowest with the AXS rotors, highest with the UNS rotor and moderate with the TCS rotors. Among the swept rotors, C_{P_rec} is reduced with increasing sweep angle. Hence the general order of decreasing C_{P_rec} is UNS, 20°TCS, 30°TCS, 20°AXS, and 30°AXS. This is true at flow coefficients above the design mass flow. At low flow coefficients, stators with highly swept rotors showed higher recoveries. Hence the order of decreasing C_{P_rec} at this lowest flow coefficient ϕ = 0.50 is UNS, 30°TCS, 20°TCS, 30°AXS, and 20°AXS. This indicates that at low flow coefficients, employing high sweep angles would leave the flow with high level of "recoverable dynamic head".

5. Summary and Conclusions

Results of the detailed computational investigation with three different sweep configurations are presented.

When the blades are given forward sweep (TCS as well as AXS) they are found to receive the flow at lower incidences. This is true all over the span for the axial sweeping while tip chordline sweeping is observed to result in little higher incidences below the mid span. As anticipated, forward sweeping resulted in minimizing the severity of flow separation at the suction surface—casing wall corners of the blades. Forward sweep is observed to lessen the flow turning by the aerofoil sections. In spite of the low flow turning, higher pressure rise seen with AXS rotors indicate efficient energy transfer with AXS rotors, which is confirmed from the study of relative stagnation pressure loss coefficients. Forward sweep (TCS) resulted in deflecting the flow towards hub while effective positive dihedral induced with axial sweeping resulted in outward deflection of flow streamlines. Streamline curvature effects due to sweep are found to be more at lower mass flow rates.

Nomenclature

ch: Chord (m)
C_m: Axial velocity (m/s)
C_r: Radial velocity (m/s)
C_u: Tangential velocity (m/s)
F_r: Radial blade force per unit mass (N/kg)
i: Incidence (deg)
LE: Leading edge
P: Pressure (N/m^2)
r: Radius (m)
r_c: Radius of curvature (m)
r/r_t: Radius ratio
TE: Trailing edge
U_t: Tip speed (m/s)
α: Absolute flow angle (deg)
β: Pitch angle (rad)

ε: Deflection (deg)
ρ: Density (kg/m^3)
τ: Tip gap (m)
ϕ : Flow coefficient (C_m / U_t)
$\psi_\circ$: Total pressure coefficient,$[\psi_\circ = ((P_{o2} - P_{o1})/\rho U_t^2)]$.

Subscripts

1: Inlet to rotor
2: Exit of rotor
3: Exit of stator
t: Tip.

Superscripts

$*$: Design conditions
$-$: Circumferentially mass averaged
$=$: Circumferentially and radially mass averaged.

References

[1] K. P. Mohammed and D. P. Raj, "Investigation on axial flow fan impellers with forward swept blades," ASME paper no. 77-FE-1, 1977.

[2] A. R. Wadia, P. N. Szucs, and D. W. Crall, "Inner workings of aerodynamic sweep," *Journal of Turbomachinery*, vol. 120, no. 4, pp. 671–682, 1998.

[3] C. Hah, S. L. Puterbaugh, and A. R. Wadia, "Control of shock structure and secondary flow field inside transonic compressor rotors through aerodynamic sweep," in *Proceedings of the International Gas Turbine & Aeroengine Congress & Exhibition*, pp. 1–15, Stockholm, Sweden, June 1998, ASME 98-GT-561.

[4] M. Govardhan, O. G. Krishna Kumar, and N. Sitaram, "Computational study of the effect of sweep on the performance and flow field in an axial flow compressor rotor," *Proceedings of the Institution of Mechanical Engineers, Part A*, vol. 221, no. 3, pp. 315–329, 2007.

[5] T. Sasaki and F. Breugelmans, "Comparison of sweep and dihedral effects on compressor cascade performance," *Journal of Turbomachinery*, vol. 120, no. 3, pp. 454–464, 1998.

[6] N. Yamaguchi, T. Tominaga, and J. Masutani, "Performance improvement by forward—skewed blading of axial fan moving blades," in *Proceedings of the 11th International Symposium on Air Breathing Engines (ISABE '93)*, pp. 580–589, Tokyo, Japan, 1993, ISABE 93-7055.

[7] G. S. McNulty, J. J. Decker, B. F. Beacher, and S. A. Khalid, "The impact of forward swept rotors on tip clearance flows in subsonic axial compressors," *Journal of Turbomachinery*, vol. 126, no. 4, pp. 445–454, 2004.

[8] L. H. Smith Jr. and H. Yeh, "Sweep and dihedral effects in axial-flow turbomachinery," *Journal of Basic Engineering*, vol. 85, no. 3, pp. 401–416, 1963.

[9] J. D. Denton and L. Xu, "The exploitation of three-dimensional flow in turbomachinery design," *Proceedings of the Institution of Mechanical Engineers, Part C*, vol. 213, no. 2, pp. 125–137, 1999.

[10] G. Pullan and N. W. Harvey, "Influence of sweep on axial flow turbine aerodynamics at midspan," *Journal of Turbomachinery*, vol. 129, no. 3, pp. 591–598, 2007.

[11] A. Fischer, W. Riess, and J. R. Seume, "Performance of strongly bowed stators in a four-stage high-speed compressor," *Journal of Turbomachinery*, vol. 126, pp. 333–338, 2004.

[12] P. V. Ramakrishna and M. Govardhan, "Combined effects of forward sweep and tip clearance on the performance of axial flow compressor stage," in *Proceedings of the ASME Turbo Expo*, Orlando, Fla, USA, 2009, GT2009-59840.

[13] S. J. Gallimore, J. J. Bolger, N. A. Cumpsty, M. J. Taylor, P. I. Wright, and J. M. M. Place, "The use of sweep and dihedral in multistage axial flow compressor blading—part 1: university research and methods development," *Journal of Turbomachinery*, vol. 124, no. 4, pp. 521–532, 2002.

[14] H. B. Squire and K. G. Winter, "The secondary flow in a cascade of aerofoils in a non-uniform stream," *Journal of the Aerospace Sciences*, vol. 18, no. 4, pp. 271–277, 1951.

[15] R. I. Lewis and J. M. Hill, "Influence of sweep and dihedral in turbomachinery blade rows," *Journal of Mechanical Engineering Science*, vol. 13, no. 4, pp. 266–285, 1971.

[16] S. A. Gbadebo, N. A. Cumpsty, and T. P. Hynes, "Three-dimensional separations in axial compressors," *Journal of Turbomachinery*, vol. 127, no. 2, pp. 331–339, 2005.

[17] M. Soundranayagam and R. L. Elder, "A study of stall in a low hub-tip ratio fan," *Journal of Turbomachinery*, vol. 115, no. 1, pp. 10–18, 1993.